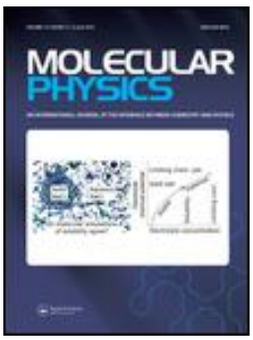

Taylor & Francis
Taylor & Francis Group

Molecular Physics

An International Journal at the Interface Between Chemistry and Physics

ISSN: 0026-8976 (Print) 1362-3028 (Online) Journal homepage: http://www.tandfonline.com/loi/tmph20

An efficient basis set representation for calculating electrons in molecules

Jeremiah R. Jones, François-Henry Rouet, Keith V. Lawler, Eugene Vecharynski, Khaled Z. Ibrahim, Samuel Williams, Brant Abeln, Chao Yang, William McCurdy, Daniel J. Haxton, Xiaoye S. Li & Thomas N. Rescigno

To cite this article: Jeremiah R. Jones, François-Henry Rouet, Keith V. Lawler, Eugene Vecharynski, Khaled Z. Ibrahim, Samuel Williams, Brant Abeln, Chao Yang, William McCurdy, Daniel J. Haxton, Xiaoye S. Li & Thomas N. Rescigno (2016) An efficient basis set representation for calculating electrons in molecules, Molecular Physics, 114:13, 2014-2028, DOI: 10.1080/00268976.2016.1176262

To link to this article: http://dx.doi.org/10.1080/00268976.2016.1176262

Published online: 27 Apr 2016.

MOLECULAR PHYSICS, 2016
VOL. 114, NO. 13, 2014–2028
http://dx.doi.org/10.1080/00268976.2016.1176262

Taylor & Francis
Taylor & Francis Group

RESEARCH ARTICLE

An efficient basis set representation for calculating electrons in molecules

Jeremiah R. Jones[e,†], François-Henry Rouet[a], Keith V. Lawler[b], Eugene Vecharynski[a], Khaled Z. Ibrahim[a], Samuel Williams[a], Brant Abeln[c,d,e], Chao Yang[a], William McCurdy[c,d,e], Daniel J. Haxton[d,e], Xiaoye S. Li[a] and Thomas N. Rescigno[e]

[a]Computing Sciences, Lawrence Berkeley National Laboratory, Berkeley, CA, USA; [b]Department of Chemistry, University of Nevada-Las Vegas, Las Vegas, NV, USA; [c]Department of Chemistry, University of California, Davis, Davis, CA, USA; [d]Ultrafast X-Ray Science Laboratory, Lawrence Berkeley National Laboratory, Berkeley, CA, USA; [e]Chemical Sciences, Lawrence Berkeley National Laboratory, Berkeley, CA, USA

ABSTRACT

The method of McCurdy, Baertschy, and Rescigno, J. Phys. B, **37**, R137 (2004) [1] is generalised to obtain a straightforward, surprisingly accurate, and scalable numerical representation for calculating the electronic wave functions of molecules. It uses a basis set of product sinc functions arrayed on a Cartesian grid, and yields 1 kcal/mol precision for valence transition energies with a grid resolution of approximately 0.1 bohr. The Coulomb matrix elements are replaced with matrix elements obtained from the kinetic energy operator. A resolution-of-the-identity approximation renders the primitive one- and two-electron matrix elements diagonal; in other words, the Coulomb operator is local with respect to the grid indices. The calculation of contracted two-electron matrix elements among orbitals requires only O(Nlog (N)) multiplication operations, not O(N^4), where N is the number of basis functions; $N = n^3$ on cubic grids. The representation not only is numerically expedient, but also produces energies and properties superior to those calculated variationally. Absolute energies, absorption cross sections, transition energies, and ionisation potentials are reported for 1- (He^+, H_2^+), 2- (H_2, He), 10- (CH_4), and 56-electron (C_8H_8) systems.

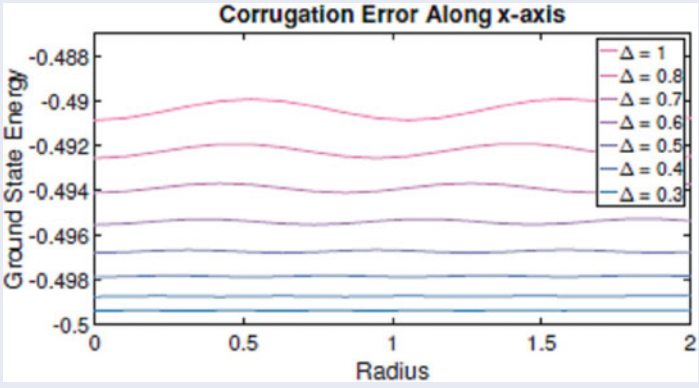

ARTICLE HISTORY
Received 5 February 2016
Accepted 1 April 2016

KEYWORDS
Sinc function; basis set; electronic structure; resolution-of-the-identity

1. Introduction

The inherent problem in scaling electronic structure methods to larger systems is the prohibitive cost of storing and transforming two-electron matrix elements, which we denote in chemists' notation

$$[ij|kl] = \int\int d^3\vec{r}_1 d^3\vec{r}_2 \; \chi_i(\vec{r}_1)\chi_j(\vec{r}_1)\frac{1}{|\vec{r}_1 - \vec{r}_2|}\chi_k(\vec{r}_2)\chi_l(\vec{r}_2) \quad (1)$$

for a basis $\{\chi_i\}$. The set of two-electron matrix elements is a fourth-rank tensor, such that transformations of the set require O(N^4) multiplication operations; sophisticated methods such as coupled cluster must cope with even poorer scaling, O(N^6). There has been much work to circumvent this basic problem [2–6], especially by Martinez and coworkers.

We describe a basis set method for electronic structure motivated by the discrete variable representation (DVR) [7–17] that is an adaptation of the method in Ref. [1]

CONTACT Jeremiah R. Jones jrjones8@asu.edu
†Present address: *Department of Mathematics, Arizona State University, Tempe, AZ 85287.*

to Cartesian coordinates. Starting with an evenly spaced grid basis means that the number of basis functions is large, but also that the rank of the two-electron matrix element tensor is automatically reduced from four to three due to redundancy. Going further, using the generalisation of Ref. [1], we obtain a diagonal two-electron matrix element tensor – in other words, we further reduce the tensor to the minimum rank one,

$$[ij|kl] \sim \delta_{ij}\delta_{kl}\, v_{i-k}. \tag{2}$$

(In this equation, the indices *i*,*j*,*k*, and *l* each would run from 1 to $N = n^3$ on a cubic grid.)

Using this resolution-of-the-identity approximation for the treatment of the Coulomb potential within the DVR, and employing established Fourier methods for triple Toeplitz linear algebra [18,19], the computation of two-electron matrix elements among molecular orbitals takes $O(N\log(N))$ time, not $O(N^4)$. The method is, therefore, not quite 'linear-scaling', but it is numerically exact; it does not involve any truncated sums in a multipole expansion, for instance.

Gaussian basis sets have traditionally been the preferred single-electron representation for real-space electronic structure calculations, due to the localised nature of these functions and the speed with which matrix elements among them may be evaluated. Although Gaussians have been widely successful, they have inherit limitations in their flexibility; in particular, they are unable to represent electrons in the continuum for nonpertubative applications. Furthermore, it is not always clear exactly how to obtain rigorous error bounds of basis set truncation.

There has recently been an increased interest among researchers in the field to develop grid-based methods using strictly numerical techniques that can handle a wider variety of problems and can be subjected to systematic error analysis. A thorough review of grid methods in electronic structure can be found in [20]. Some examples of grid-based techniques currently in use are finite differences [21–23], finite elements [24,25] and wavelets [26]. These methods make the treatment of arbitrary boundary conditions considerably easier than basis set methods. Another advantage of grid methods is the flexibility allowed in performing calculations on complicated spatial domains. Finite difference methods are limited in this regard since they require strictly rectangular meshes, whereas finite element methods offer complete freedom in choosing a computational mesh.

Similar to finite element methods, DVR methods have characteristics of both a basis set method and a grid method in the sense that each basis function is localised around a specific grid point, and potential functions are evaluated as local multiplicative operators on the grid. Many DVR bases have appeared in the literature, including those based on Bessel functions [16] Lagrange polynomials [27,28], and sinc functions [29–31], as well as multidimensional bases [15] and others described in Refs. [7–17].

One issue in evaluating potential energy matrix elements for molecular systems is how to resolve the singularities that occur in the Coulomb potential terms. A number of methods for doing so have appeared in the literature, including the use of energy cut-off functions [32,33] and multipole expansions via Legendre polynomials in spherical coordinates [1,34]. The singular Coulomb potential cannot be used straightforwardly within the DVR approximation, because doing so would entail the use of infinite diagonal matrix elements.

To address this issue, the present method makes use of the fact that the Green's function for the Laplace operator is the Coulomb potential. In doing so, it follows the derivation used in Ref. [1]. That work presented a treatment in spherical polar coordinates, using the partial-wave expansion of the Green's function, arriving at expressions for the two electron matrix elements diagonal in the radial index, corresponding to an expansion in Gauss–Lobatto DVR for the radial degree of freedom. Here, we do not use the partial-wave expansion and instead treat Poisson's equation in Cartesian coordinates.

We present the method in the next section, then results, and finally in the conclusion we speculate about possible elaborations to the method that could make it more versatile for excited state and time-dependent problems, and perhaps even competitive with Gaussian basis sets for the computation of results requiring chemical accuracy [35].

2. Method

2.1. Sinc basis

Sinc functions have been used extensively in several areas of applied mathematics including numerical solutions to ordinary and partial differential equations, interpolation and Fourier analysis [36] but were first introduced in the context of a DVR basis for solving the Schrödinger equation by Colbert and Miller in [29]; a good description of the sinc DVR can also be found in Ref. [37]. Sinc basis functions have been used in electronic structure in Refs. [29–31].

The sinc function is defined as

$$\mathrm{sinc}(x) = \begin{cases} \dfrac{\sin(\pi x)}{\pi x} & \text{if } x \neq 0 \\ 1 & \text{if } x = 0 \end{cases}. \tag{3}$$

and an orthonormal basis in one dimension is

$$\xi_i(x) = \frac{1}{\sqrt{\Delta}}\mathrm{sinc}\left(\frac{x - x_i}{\Delta}\right) \tag{4}$$

with Δ the uniform grid spacing, $x_{i+1} = x_i + \Delta$. We make a three-dimensional (3D) product basis in the straightforward way,

$$\chi_{\vec{i}}(x, y, z) = \xi_{i1}(x)\xi_{i2}(y)\xi_{i3}(z). \tag{5}$$

2.2. Kinetic energy matrix elements

The kinetic energy matrix elements for the one-dimensional (1D)basis are

$$\begin{aligned} t_{ij} &= \left\langle \xi_i \middle| -\frac{1}{2}\frac{d^2}{dx^2} \middle| \xi_j \right\rangle \\ &= \begin{cases} \pi^2/(6\Delta^2) & \text{if } i = j \\ (-1)^{i-j}/(\Delta^2(i-j)^2) & \text{if } i \neq j \end{cases}. \end{aligned} \tag{6}$$

Notice that these matrix elements only depend on $i - j$, i.e. t is constant along diagonals, i.e. t is Toeplitz. A derivation of these elements is given in Ref. [29]. It is interesting to note that these matrix elements form an exact representation of the kinetic energy operator projected onto the grid and can be derived in the limit of an infinite-order finite difference scheme, independent of any underlying basis set.

The 3D kinetic energy elements are

$$T_{\vec{i}\vec{j}} = t_{i1,j1}\delta_{i2,j2}\delta_{i3,j3} + \delta_{i1,j1}t_{i2,j2}\delta_{i3,j3} + \delta_{i1,j1}\delta_{i2,j2}t_{i3,j3}. \tag{7}$$

Since t and the identity matrix are Toeplitz, T is triple Toeplitz, as are the matrix elements of any translationally invariant operator. We only use explicit vector-index notation in Equations (5) and (7), and in Sections 2.6 and 2.7. In the rest of this paper, we use contracted indices, such that for a 3D basis function $\chi_i(\vec{r})$, or matrix element T_{ij}, the index i (or j) represents a single integer that runs from 1 to $N = n^3$ on a cubic grid.

2.3. Discrete variable representation resolution of the identity for two-electron matrix elements

In the generalisation of Ref. [1] to Cartesian coordinates, there are several simplifications that result from the use of sinc basis functions. The present method and that of Ref. [1] are founded on the replacement of Coulomb matrix elements by matrix elements obtained from the kinetic energy operator via a resolution-of-the identity approximation invoking Poisson's equation. However, for the two-electron matrix elements, it is not necessary to introduce the kinetic energy operator into the derivation, if the sinc DVR is used. Therefore, in this section, we provide the simplest derivation of the two-electron matrix elements used in this method, before introducing the kinetic energy operator in the sections below.

The method of Ref. [1] uses the fact that the Coulomb potential is the Green's function of the Laplace operator to avoid the inherent problem with using the DVR approximation for singular potentials. It results in an expression, Equation (24), which for the sinc DVR basis is equivalent to the resolution of the identity described in this section:

$$[ij|kl] = 2\pi\delta_{ij}\delta_{kl}(w_i w_j)^{-\frac{1}{2}}T^{-1}_{ik}$$

where the w are the quadrature weights – presently, for the 3D Cartesian sinc basis uniformly equal to Δ^3 – and T^{-1} is the limit of the inverse of the kinetic energy matrix as the size of the basis is taken to be infinity. Because the sinc basis is complete in momentum space up to a cut-off, the matrix element of the matrix inverse is equal to the matrix element of the operator inverse,

$$(T^{-1})_{ik} = \int d^3r_1 d^3r_2\ \chi_i(\vec{r}_1)\frac{1}{2\pi|\vec{r}_{12}|}\chi_k(\vec{r}_2)\ . \tag{8}$$

Because Equation (8) holds for the sinc DVR basis, there is no need to introduce the kinetic energy matrix into the derivation of the two-electron matrix elements. Our final expression for them, Equation (12), results simply from a resolution-of-the-identity approximation.

The resolution of the identity makes straightforward use of the interpolating property of DVR basis functions: each basis function belongs to a grid index, and is zero at all the grid points other than that corresponding to its own index. This 'discrete orthogonality' condition [38] is the defining property of a DVR basis set. An arbitrary function can be expanded easily in such an interpolating basis,

$$f(x) \approx (w_i)^{-1/2}\sum_i \chi_i(x)f(x_i) \tag{9}$$

where w_i is the quadrature weight at point i; presently, the weights are all equal to Δ for the 1D sinc DVR and Δ^3 for the 3D product basis. This may be written as a resolution of the identity,

$$f(x) \approx \sum_i |\chi_i\rangle\langle\chi_i|\ f(x) \tag{10}$$

where the integral is performed using the underlying quadrature, giving

$$\chi_k(\vec{r})\chi_l(\vec{r}) \approx \delta_{kl}(w_k)^{-1/2}\chi_k(\vec{r}) \tag{11}$$

such that the density (a sum of squares of localised basis functions) is re-expanded as a sum of localised basis functions, without the square. The fact that the auxiliary basis, the one in which the density is expanded, is the same as the basis in which the wave function is resolved means that, at least aesthetically, it is the *ideal* resolution of the identity.

The expression for the two-electron integral is obtained simply from Equations (1) and (11),

$$[\vec{ij}|\vec{kl}] \approx \Delta^{-3}\delta_{ij}\delta_{kl}\int d^3r_1 d^3r_2\ \chi_i(\vec{r}_1)\frac{1}{|\vec{r}_{12}|}\chi_k(\vec{r}_2) \tag{12}$$

2.4. Application of the method of Ref. [1] to arbitrary three-dimensional discrete variable representations

Here, we provide a derivation of both the one- and two-electron matrix elements that follows the derivation in Ref. [1] closely. This method is founded upon the observation that the Coulomb potential is the Green's function of the kinetic energy (Laplace) operator, and replaces Coulomb matrix elements in a basis with matrix elements obtained from the kinetic energy operator in the same basis. There are only two significant differences between the derivation in Ref. [1] and this one: one, we use the full 3D Green's function for the Laplacian operator, not its partial wave expansion; and two, we eliminate the need for an explicit boundary condition. For sinc basis functions, the derivation of the two-electron matrix elements may be simplified as in the section above, but the derivation here is applicable to general DVRs in three dimensions and includes both the one- and two-electron matrix elements. An extension of this derivation is presented in Appendix A, which derives the matrix elements for electrons defined on different grids.

We define

$$y^{kl}(\vec{r}_1) = \int d^3\vec{r}_2\ \chi_k(\vec{r}_2)\chi_l(\vec{r}_2)\frac{1}{|\vec{r}_1 - \vec{r}_2|} \tag{13}$$

so that, with reference to Equation (1), we can write

$$[ij|kl] = \int d^3\vec{r}_1\ \chi_i(\vec{r}_1)\chi_j(\vec{r}_1)y^{kl}(\vec{r}_1). \tag{14}$$

Applying the Laplacian to both sides of Equation (13) results in the Poisson equation

$$\nabla^2_{\vec{r}_1} y^{kl}(\vec{r}_1) = -4\pi\,\chi_k(\vec{r}_1)\chi_l(\vec{r}_1). \tag{15}$$

Here, we have used the fact that

$$G(\vec{r},\vec{r}') \equiv -\frac{1}{4\pi|\vec{r}-\vec{r}'|} \tag{16}$$

is the free space Green's function for the Laplace operator satisfying

$$\nabla^2_{\vec{r}} G(\vec{r},\vec{r}') = \delta(\vec{r}-\vec{r}') \tag{17}$$

with the boundary condition $G(\vec{r},\vec{r}') \to 0$ as $|\vec{r}| \to \infty$. We now approximate $y^{kl}(\vec{r}_1)$ as a linear combination of the basis functions,

$$y^{kl}(\vec{r}_1) \approx \sum_{\text{ALL } n} y^{kl}_n \chi_n(\vec{r}_1), \tag{18}$$

with an infinite sum over the product basis functions covering all space. In numerical calculations, a finite basis is always used, but by including all possible product basis functions in the above sum we avoid the need for a boundary condition term, as was needed (and easily handled) in the prior treatment in spherical polar coordinates [1]. Applying the Laplacian with respect to $\vec{r}_1$ to this expansion gives

$$\nabla^2_{\vec{r}_1} y^{kl}(\vec{r}_1) \approx \sum_{\text{ALL } n} y^{kl}_n \nabla^2_{\vec{r}_1}\chi_n(\vec{r}_1). \tag{19}$$

Multiplying Equations (15) and (19) through by $\chi_m(\vec{r}_1)$, integrating over $\vec{r}_1$ and equating the results leads to

$$\sum_{\text{ALL } n} y^{kl}_n T_{mn} = 2\pi\int d^3\vec{r}\chi_k(\vec{r})\chi_l(\vec{r})\chi_m(\vec{r}) \tag{20}$$

where $T_{mn} = -\frac{1}{2}\langle\chi_m|\nabla^2|\chi_n\rangle$ are the kinetic energy matrix elements.

The integral on the right-hand side of Equation (20) is evaluated by a resolution of the identity, Equation (11), such that the density (a sum of squares of localised basis functions) is re-expanded as a sum of localised basis functions, without the square. From Equations (20) and (11),

$$\sum_{\text{ALL } n} y^{kl}_n T_{mn} = 2\pi\,\delta_{kl}\delta_{lm}(w_k w_l)^{-1/2} \tag{21}$$

giving

$$y^{kl}_n = 2\pi\,\delta_{kl}(w_k)^{-1}(T^{-1})_{nk}, \tag{22}$$

where T^{-1} is the limit of the matrix inverse as the size of the matrix goes to infinity. Using these coefficients and inserting Equation (18) into Equation (14) gives

$$[ij|kl] = \sum_n y_n^{kl} \int d^3\vec{r}_1 \; \chi_i(\vec{r}_1)\chi_j(\vec{r}_1)\chi_n(\vec{r}_1). \tag{23}$$

Once again, the integral on the right-hand side is evaluated by resolving the identity and employing DVR quadrature to obtain the final expression for the two electron matrix elements

$$[ij|kl] = 2\pi\delta_{ij}\delta_{kl}(w_i w_k)^{-1/2} T^{-1}_{ik}. \tag{24}$$

2.5. One-electron matrix element

The expression for the one-electron matrix element for a nucleus at position $\vec{R}$, here denoted U_{ij},

$$U_{ij}(\vec{R}) \equiv \left\langle i \left| \frac{1}{|\vec{r} - \vec{R}|} \right| j \right\rangle \tag{25}$$

within the present method follows simply from the analog of Equation (18),

$$U_{ij}(\vec{R}) \approx \sum_{\text{ALL } n} u_n^{ij} \chi_n(\vec{R}); \tag{26}$$

Equation (11), which is the resolution of the identity approximation; and Poisson's equation:

$$\nabla^2_{\vec{R}} U_{ij}(\vec{R}) = 4\pi\,\chi_i(\vec{R})\chi_j(\vec{R}) \approx 4\pi\,\Delta^{-3/2}\delta_{ij}\chi_i(\vec{R}) \tag{27}$$

within the weak variational formulation, i.e. multiplying by the left by $\int d^3R \; \chi_k(\vec{R})$ for all k. The one-electron matrix element is thereby simply related to the two-electron matrix element,

$$U_{ij}(\vec{R}) \approx y^{ij}(\vec{R}); \tag{28}$$

both are defined via Equations (18) and (22) in terms of the kinetic energy matrix elements. However, we find that accurate results are only obtained when the nuclei are at positions $\vec{R}$ coinciding with electronic DVR grid points $\vec{r}_i$. In other words, for the moment, the method requires that the nuclei be placed on the Cartesian grid points, which is a major limitation. We do not understand this behaviour and comment upon it, and ways to avoid it, in the conclusion.

In order to use the above expressions in a practical way, for general DVR bases, we must have a method of approximating the matrix elements of T^{-1}. However, simply inverting the finite-dimensional kinetic energy matrix is not a good approximation and would also require the storage of a dense matrix, which is impractical for even modestly sized grids. We use the method below, which directly calculates the entire set of diagonal two-electron matrix elements at one time, and which would be applicable to other generalised DVR basis sets besides the Cartesian product sinc functions used here.

2.6. Kinetic energy inverse

The key to a practical implementation is to consider the representation of T^{-1} on an infinite grid, and then truncate the matrix elements to a finite grid. The full kinetic energy in three dimensions is given in Equation (7). Since t is Toeplitz, T is Toeplitz with respect to each of the spatial indices, i.e. T is triple Toeplitz, and therefore it could be denoted using a symbol with only one three-vector index, e.g. $T_{\vec{i}\vec{j}} = u_{\vec{i}-\vec{j}}$. (In this subsection, we momentarily revert to explicit vector index notation.) Its inverse inherits this property,

$$(T^{-1})_{\vec{i}\vec{j}} = v_{\vec{i}-\vec{j}} \tag{29}$$

The expression $TT^{-1} = 1$ can be rewritten

$$(u * v)_{\vec{j}} \equiv \sum_{\vec{i}=-\infty,\infty,\infty}^{\infty,\infty,\infty} u_{\vec{i}-\vec{j}} v_{\vec{i}} = \delta_{j1,0}\delta_{j2,0}\delta_{j3,0} \tag{30}$$

where $*$ represents the discrete convolution product.

For the sinc DVR, we may derive an exact expression for the matrix element amenable to quadrature, but instead we solve for all of the matrix elements simultaneously using the following method, which is also applicable to other bases. The strategy is to take the lowest-order Taylor series expression for the matrix element, for those matrix elements at long range, and solve for the remainder.

Thus, we approximate the matrix elements of T^{-1} between basis functions far separated as

$$v_{\vec{i}} \xrightarrow{|i|\to\infty} \frac{\Delta^3}{2\pi}\frac{1}{r_{\vec{i}}} = \frac{\Delta^2}{2\pi}\frac{1}{\sqrt{i_1^2 + i_2^2 + i_3^2}} \tag{31}$$

such that $[ij|kl] \longrightarrow \delta_{ij}\delta_{kl}\frac{1}{r_{i-k}}$. We assume that Equation (31) holds exactly for three-indices $\vec{i}$ in which i_1, i_2, or i_3 is greater than n_{small}, where n_{small} is an adjustable parameter, and solve Equation (30) for the remainder of v. In other words, we solve

$$\sum_{\vec{i}=-n_{big},n_{big},n_{big}}^{n_{big},n_{big},n_{big}} u_{\vec{i}-\vec{j}} v_{\vec{i}} = \delta_{j1,0}\delta_{j2,0}\delta_{j3,0} \tag{32}$$

given $u_{\vec{i}-\vec{j}} = T_{\vec{i}\vec{j}}$ and

$$v_{\vec{i}} = \frac{\Delta^2}{2\pi}\frac{1}{\sqrt{i_1^2+i_2^2+i_3^2}} \qquad \begin{pmatrix} |i_1| > n_{\text{small}} \text{ or} \\ |i_2| > n_{\text{small}} \text{ or} \\ |i_3| > n_{\text{small}} \end{pmatrix} \tag{33}$$

for the remaining $(2n_{\text{small}}+1)^3$ elements of v. The infinite sum in Equation (30) is truncated at n_{big} and we, therefore, have two convergence parameters, n_{small} and n_{big} defining the approximated T^{-1}. We have chosen a default of 40 and 240 for these numbers, respectively, and we verify the convergence as a function of these parameters of all the results presented below.

2.7. Triple Toeplitz linear algebra with Fourier transforms

We continue with vector index notation in this section, after which we revert to condensed index notation.

To construct a two-electron matrix element among contracted basis functions

$$\phi_\alpha(\vec{r}) = \sum_{\vec{i}} c_{\vec{i}\alpha}\chi_{\vec{i}}(\vec{r}) \tag{34}$$

we must perform the sum

$$[\alpha\beta|\gamma\delta] = \sum_{\vec{i}\vec{k}} 2\pi\,(w_{\vec{i}}w_{\vec{k}})^{-1/2} v_{\vec{i}-\vec{k}} c^*_{\vec{i}\alpha} c_{\vec{i}\beta} c^*_{\vec{k}\gamma} c_{\vec{k}\delta} \tag{35}$$

wherein a triple Toeplitz matrix–vector multiplication is performed by the triple Toeplitz matrix v upon the density $\phi^*_\alpha\phi_\beta$ to produce a potential that is then integrated over the density $\phi^*_\gamma\phi_\delta$, or vice versa.

The matrix T^{-1} is triple Toeplitz (a.k.a., 3-level Toeplitz), i.e.$(T^{-1})_{ijk,i'j'k'} = v_{i-i',j-j',k-k'}$ where v is a $(2l-1)\times(2m-1)\times(2n-1)$ tensor and T^{-1} is an $N\times N$ matrix with $N = lmn$. A triple Toeplitz matrix is (a) block Toeplitz, e.g.

$$T^{-1} = \begin{bmatrix} (T^{-1})_0 & (T^{-1})_1 & \cdots & (T^{-1})_n \\ (T^{-1})_{-1} & (T^{-1})_0 & \cdots & (T^{-1})_{n-1} \\ \vdots & (T^{-1})_{-1} & \ddots & \vdots \\ (T^{-1})_{-n-1} & \vdots & \ddots & (T^{-1})_1 \\ (T^{-1})_{-n} & (T^{-1})_{-n-1} & \cdots & (T^{-1})_0 \end{bmatrix}$$

Furthermore, (b) the blocks are double Toeplitz (or two-level Toeplitz), i.e. they are block Toeplitz with Toeplitz blocks (also called BTTB in the literature). Similarly, a triple circulant matrix C is such that $C_{ijk,i'j'k'} = c_{i-i'+1 \pmod l, j-j'+1 \pmod m, k-k'+1 \pmod n}$ (c is an $l\times m\times n$ tensor, C is an $N\times N$ matrix, $N = lmn$).

Triple circulant matrices are diagonalised by the 3D Fourier transform (Theorem 5.8.4 in [18]):

$$C = F'\cdot \text{diag}(Fc)\cdot F$$

An $N\times N$ triple Toeplitz matrix can be embedded into an $8N\times 8N$ triple circulant matrix [19]. Therefore, just as with single Toeplitz [39], a matrix–vector product involving a triple Toeplitz matrix, such as that required to compute two-electron matrix elements, may be computed in $O(N\log N)$ floating point operations using a fast Fourier transform, instead of $O(N^2)$. Memory use is minimal, due to the redundancy inherent in Toeplitz matrices.

The embedding that is used [19] to transform the $N\times N$ triple Toeplitz matrix into an $8N\times 8N$ triple circulant matrix consists in padding the tensor v with zeros. We summarise the algorithm:

Matrix–vector product $y = (T^{-1})x$ with $T^{-1}: N\times N$ **Triple Toeplitz matrix**, $N = lmn$, defined by $v: (2l-1)\times(2m-1)\times(2n-1)$ **tensor**	
1: $x_2 = 0$	$(2l\times 2m\times 2n)$
2: $x_2(1:l, 1:m, 1:n) = x(:,:,:)$	
3: $v_2 = 0$	$(2l\times 2m\times 2n)$
4: $v_2(2:2l, 2:2m, 2:2n) = v(:,:,:)$	
5: $f_x = \text{FFT-3D}(x_2)$	
6: $f_v = \text{FFT-3D}(v_2)$	
7: $f_y = f_x \times f_v$	(element-wise product)
8: $y_2 = \text{IFFT-3D}(f_y)$	
9: $y(:,:,:) = y_2(l+1:2l, m+1:2m, n+1:2n)$	

3. Results

In this section, we present the results of several calculations performed with the the methods previously described. We begin with calculations of energy states of some simple benchmark systems, such as He^+, H_2^+ and He. Later, we present time-dependent results for emission and absorption spectrums of methane (CH_4), as well as excitation energies of methane and the ionisation potential of cubane (C_8H_8).

3.1. DVR method vs. variational method

Remarkably, the treatment we have outlined appears to perform better than the variational method, where the integrals for the Coulomb matrix elements are evaluated directly with numerical quadrature methods. We have not been able to test the variational method for a two-electron problem with the methods available to us, due to the prohibitive cost of computing and storing matrix elements. To compare with the variational method, we just consider the single-electron helium ion He^+. All integrals were evaluated in spherical coordinates, using

Table 1. The $n = 1, 2, 3$ eigenvalues and virial theorem ratios $\langle T\rangle/\langle v\rangle$ for He^+ using both the DVR and the variational method with grid spacing $\Delta = 0.4a_0$.

	Energy			Virial theorem		
State	DVR	Variational	Exact	DVR	Var.	Ex.
1*s*	− 1.9765	− 1.9526	− 2	− 0.4939	− 0.4817	− 0.5
2*p*	− 0.4998	− 0.4953	− 0.5	− 0.4998	− 0.5184	− 0.5
2*s*	− 0.4976	− 0.4826	− 0.5	− 0.4987	− 0.5280	− 0.5
3*d*†	− 0.2189	− 0.1761	− 0.22...	− 0.5282	− 0.7108	− 0.5
3*d**	− 0.2155	− 0.1712	− 0.22...	− 0.5494	− 0.7184	− 0.5

† *xy*, *yz* and *xz* components * $2z^2 - x^2 - y^2$ and $x^2 - y^2$ components.

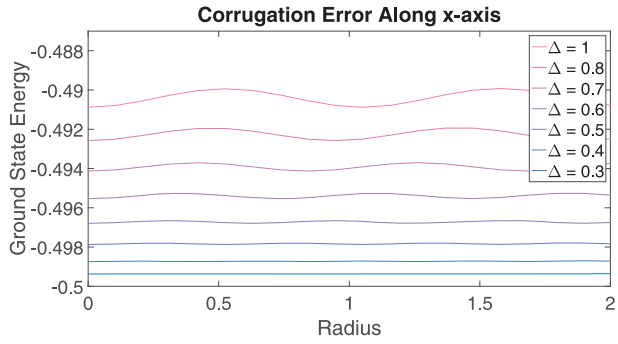

Figure 1. The ground-state energy of hydrogen as a function of nuclear position along the *x*-axis for several values of the grid spacing.

Fourier quadrature for the polar angle nodes, Gauss–Laguerre quadrature for the radial nodes and Gauss–Legendre quadrature for the azimuthal angle nodes. The number of nodes for each coordinate is automatically chosen to ensure the results are accurate to double precision.

Although the method described in this paper is technically not a variational method, all of the energies obtained by this method have always been strictly greater than the exact values and converge monotonically, with a quadratic rate, to the exact energy values as $\Delta \to 0$.

In Table 1, we show the $n = 1, 2, 3$ energy states of He^+ and the ratios $\langle T\rangle/\langle v\rangle$ for both the DVR and variational methods, using a grid spacing of $\Delta = 0.4a_0$. The present DVR method clearly gives better energies, in one case (2p) by nearly two orders of magnitude. Results for the virial theorem are even more decisive, up to three orders of magnitude. We speculate that the reason for this favourable performance is that the relationship between the Coulomb potential and the kinetic energy operator is maintained in matrix form. It is interesting that our method computes the $n = 2$ excited states to greater accuracy than the ground state, which is rather atypical. This is most likely due to the coarseness of the grid and by the slow-decaying long-range nature of sinc functions. The coarse grid does not resolve the tight 1s orbital very well and the long-range behaviour of the sinc functions make them better suited for representing the more diffuse 2p orbitals.

We also note that the improved accuracy of the p-states appears to come from the use of the DVR method itself and does not depend on our representation of T^{-1}. However, the accuracy in the s-state is more sensitive to the representation of T^{-1} and gives superior accuracy compared to the standard DVR approach. This makes sense physically given that the p-states vanish at the origin and the s-state does not. Therefore, the main advantage of our method for calculating T^{-1} is really in its ability to accurately resolve the Coulomb singularity at the origin.

3.2. Corrugation error (muffin-tin effect)

The 'muffin tin effect' is the corrugation that occurs when treating a translationally invariant problem using a fixed lattice. The one-electron operator is defined for arbitrary nuclear coordinates through overlaps of the operator bases, centred on each nucleus and the wave function basis. Because the sinc basis is complete in momentum space up to a certain cut-off, any two such complete sets, however translated relative to one another, span the same space. Therefore, the corrugation error should be eliminated by converging the calculation with respect to the extent of the grid. In other words, there should be no corrugation error independent of truncation error. Unfortunately, we do not find this is the case and currently have no explanation for this.

In Figure 1, we show the ground-state energy of hydrogen as a function of nuclear position along the *x*-axis for various values of the grid spacing. The oscillation amplitudes clearly become smaller as the grid spacing is decreased. In a more detailed test, we varied the nuclear position along different vectors and measured the maximum corrugation amplitude for several values of Δ. In Figure 2, we show a log–log plot of this maximum corrugation amplitude as a function of Δ for four different vectors. For each direction, the corrugation error appears to obeys a power law with respect to the grid spacing. We estimate that the error is proportional to Δ^p where $p \approx 3.25$.

3.3. H_2^+ Results

In Figure 3, we show the relative error in the $n = 1, 2$ energies of H_2^+ for different grid resolutions, compared with exact results obtained in prolate spheroidal coordinates as in Ref. [40]. The errors are on the order of a millihartree for $\Delta = 0.5$ and $0.8a_0$ and are 1–2 orders of magnitude better with $\Delta = 0.25a_0$. The errors are also

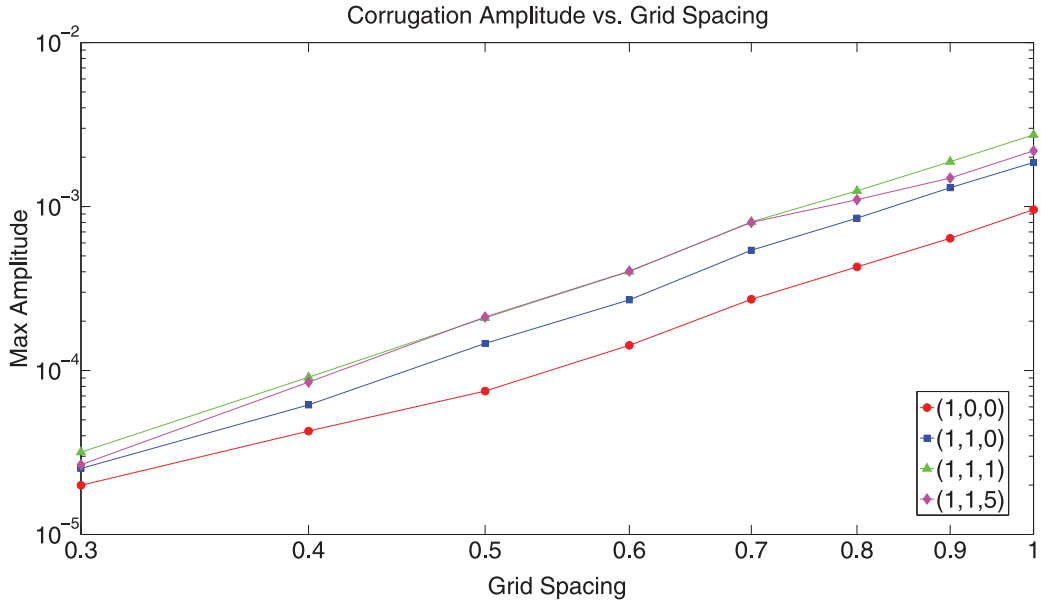

Figure 2. The maximum corrugation amplitude as a function of grid spacing. For each line shown, the nucleus position is varied along a straight line in the direction of the vector listed in the legend.

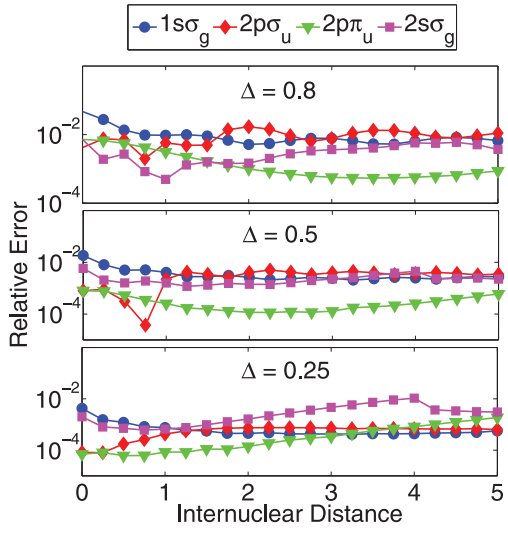

Figure 3. The relative error in the $n = 1, 2$ energies of H_2^+ vs. internuclear distance, with $\Delta = 0.25$, 0.5, and $0.8a_0$, from $R = 0$ to $5a_0$.

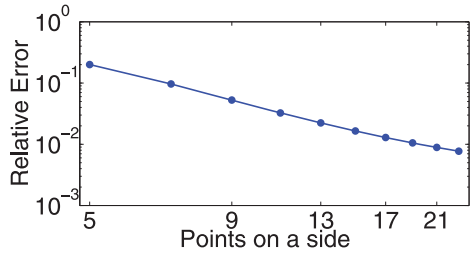

Figure 4. The relative error in the ground-state energy of He vs. the number of grid points per spatial dimension with a fixed box size of $3a_0$, plotted on a log–log scale.

relatively constant with respect to the internuclear distance. It appears that the $2p\pi_u$ state is generally more accurate than the ground state, again reflecting the long-range nature of the sinc functions.

3.4. Two-electron results

In Figure 4, we plot the relative error in the ground state of Helium for multiple grid resolutions with a fixed box size of $3a_0$, which is sufficient to eliminate truncation error. The figure demonstrates a roughly quadratic convergence rate of the ground-state energy of Helium with respect to the grid resolution; the error is proportional to N^p where $p \approx -2.13$. When applied to systems with smooth potentials, the sinc basis demonstrates exponential convergence, as any rigorous spectral method should. The quadratic convergence rate seen here is a result of the singular Coulomb potential.

In Figure 5, we show the relative error in the ground-state energy of H_2 for different grid resolutions. As expected, the results with $\Delta = 0.5a_0$ are more accurate than with $\Delta = 0.8a_0$. However, both resolutions have error roughly on the order of 10^{-2}, with the errors being slightly larger for R close to zero. Comparing the ground-state errors of H_2 with those of H_2^+, we see that the H_2 calculations are slightly less accurate, due to the error introduced by the two-electron operator.

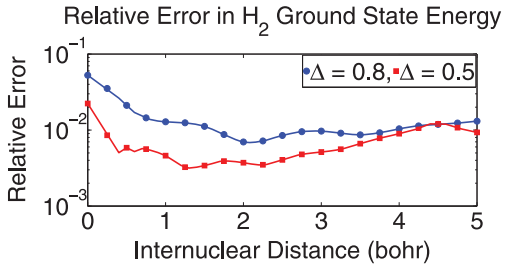

Figure 5. The relative error in the ground-state energy of H_2 vs. internuclear distance, with $\Delta = 0.5$ and $0.8a_0$, from $R = 0$ to $5a_0$, defined relative to the benchmark results of Ref. [66].

3.5. Methane photoexcitation, time-dependent calculation

We calculate time-dependent nine-orbital full configuration interaction electronic wave functions for methane using the method described in Ref. [41]. We use grid spacings Δ of 0.39495414 and 0.19747707 bohr. These spacings permit a bond length of of 1.086Å, which is the equilibrium bond length at the highest level of theory in Ref. [42]. We position hydrogen nuclei at $(x, y, z) = \{(A, A, A), (A, -A, -A), (-A, A, -A), (-A, -A, A)\}$ where $A = 3\Delta$ or $A = 6\Delta$, respectively, for the two grid resolutions. The absorption spectra are calculated in a straightforward manner, as in Ref. [43], and shown in Figure 6.

We perform three nine-orbital full-configuration-interaction calculations – 15876 Slater determinants, 5292 spin adapted singlet configurations – with different grid bases but otherwise identical, and approximately equal total wall clock computation time. Due to the different rates of calculation, different final times are reached:

- Resolution $\Delta = 0.39495414a_0$, 63 points on a side: $t_{\text{final}} \approx 7.5$fs (300 atomic units), or
- Resolution $\Delta = 0.39495414a_0$, 31 points on a side: $t_{\text{final}} \approx 24.2$fs (1000 atomic units), or
- Resolution $\Delta = 0.19747707a_0$, 63 points on a side: $t_{\text{final}} \approx 121$fs (5000 atomic units)

The difference in speed between the two 63-point calculations is due to the different behaviour of the method for the different resolution grids. The difference between the two calculations with coarse resolution is due to the size of the basis. The basis size affects the Fourier transform time ($O(n^3 \log(n))$) and the kinetic energy time ($O(n^4)$), but with a smaller coefficient).

Excitation of the low-lying valence states leads to photodissociation; photodissociation of methane has been studied by several authors [42,44–46]. The vertical excitation energy of the lowest state was calculated in Ref. [42] to be 10.60eV and this appears to be the most reliable value in the literature. We have used the same bond length as in that work.

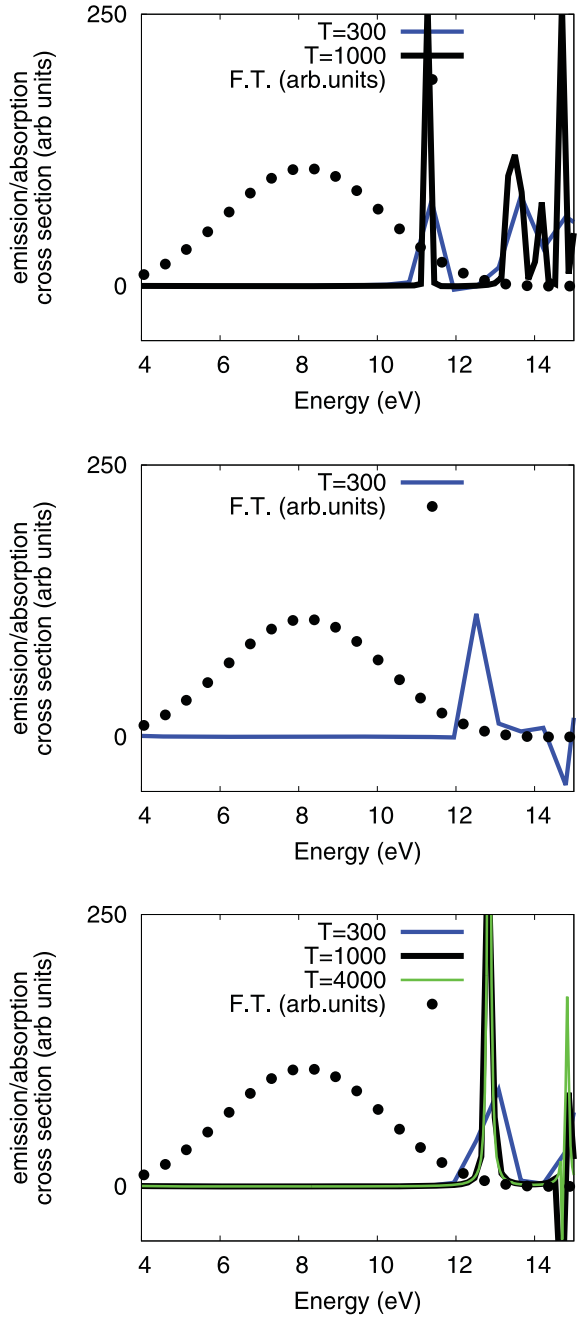

Figure 6. Bound-state absorption spectrum for methane calculated one pulse and equal wall clock computation time. Top to bottom: Grid spacing $0.39495414a_0$, 63 points on a side; grid spacing $0.39495414a_0$, 31 points on a side; grid spacing $0.19747707a_0$, 63 points on a side. Time is in atomic units; divide by 41.34 for femtoseconds.

One can see that, of the three panels shown in Figure 6, the first one shows a peak that is just above 11eV, whereas the peak in the other panels occurs higher, between 12 and 13eV. The difference is due to the truncation error, the error caused by insufficient spatial extent of the grid; the grid used for the top panel is about twice as wide as that used for the other two. The difference between the

middle and bottom panels in this figure is due to resolution. The grids have approximately the same extent in these figures, but the bottom figure uses a grid spacing $\Delta \approx 0.2a_0$, whereas the middle uses $\Delta \approx 0.4a_0$. The difference in the $t = 300$ curves on the middle and bottom panels is minor. So we see that a box size of $24a_0$ and a grid spacing of $0.4a_0$ are probably sufficient for calculations of excited state physics on methane.

The fact that we must use a large basis set to represent electronic wave functions with large spatial extent is certainly a problem with the representation, and we comment on the possibility of stretching the grid in the asymptotic region later, in the conclusion. We would like to avoid truncation error, what comes from a grid of insufficient spatial extent, in the analysis of this basis set method, and focus on resolution error. In Subsections 3.7 and 3.8, we perform apples-to-apples comparisons of the sinc DVR to Gaussian basis sets, in which we eliminate truncation error, which does not apply to Gaussian basis sets, from consideration. The method we use for this purpose is described below.

3.6. Method for extrapolation to infinite grid size

Below, we report transition energies and ionisation potentials for polyatomic molecules. The desire is to present the results without error due to the use of a grid with finite extent. The 'truncation error', the error due to having an insufficient number of points on a side n, is uninteresting and should be eliminated.

The resolution error, in contrast, is of prime importance. We have conjectured that this is an ideal smoothed Coulomb representation on a Cartesian grid. So we report numbers that are functions of resolution Δ, but not of points on a side n. However, they have error bars due to the method used to extrapolate them, as a function of points on a side n, to $n = \infty$. We report excitation energies as a function of resolution Δ, with error bars due to truncation error in our finite basis calculations. The method we use to extrapolate the energies is ad hoc and is as follows.

We choose a function $f(n; \vec{P})$ that is monotonic as a function of n and that approaches a limit as $n \longrightarrow \infty$ but that is otherwise arbitrary, and that is a function not only of n but also of certain number N_P of parameters P_i, $i = 1 \ldots N_P$. Each eigenvalue $E_\alpha(n), \alpha = 1 \ldots 12$ is fit separately as a function of n to the function f by varying the parameters of f.

The uncertainty in the extrapolated energy eigenvalue will be affected by the choice of f. We regard f as unknown and seek to find one that provides acceptable precision in the reported extrapolated eigenvalue. Presently, we have tried functions of the form $P_1 + P_2 n^Q e^{-nP_3}$ and find that

$$f(n; P_1, P_2, P_3) = P_1 + P_2 n^2 e^{-nP_3} \tag{36}$$

gives a consistently superior fit to the present data, when compared to the other choices we tried with $Q \neq 2$, so we chose this function, with an n^2 factor in the exponential term, for f. We perform a least squares regression, choosing N_C values of n with which to perform calculations and minimising

$$\forall_{\alpha=1\ldots12, i=1\ldots N_P} \frac{\partial}{\partial P_{\alpha i}} \sum_{j=1}^{N_C} \left[E_\alpha(n_j) - f(n_j; \vec{P}_\alpha)\right]^2 = 0 \tag{37}$$

The predicted asymptote is the first parameter, P_1 from Equation (36), the constant term,

$$E_\alpha(\infty) \equiv P_1 \tag{38}$$

The variance in the predicted $E_\alpha(\infty)$ will be denoted σ_α^2. There is systematic error in the prediction due to the lack of knowledge about the exact form of the unknown function f. There is statistical error due to imperfect convergence of the calculated eigenvalues $E_\alpha(n)$. So we estimate the variance as

$$\sigma_\alpha^2 = \left(\sigma_\alpha^{\text{sys}}\right)^2 + \left(\sigma_\alpha^{\text{stat}}\right)^2 \tag{39}$$

with the systematic error defined as the asymptotic standard error of the parameter P_1.

The statistical error for each computed eigenvalue $E_\alpha(n)$ is that caused by imperfect convergence of the MCTDHF relaxation procedure. We have a primitive implementation but choose a stringent convergence criterion. The change in energy between the penultimate and final iterations, which we will denote $\Delta E_\alpha(n)$, is generally less than one microhartree, and this number is recorded for each eigenvalue and used to estimate $\sigma_\alpha^{\text{stat}}$. We performed several small runs with an error criterion even more stringent. We estimate that the change in energy between the penultimate and final iterations is significantly more than 100 times the error in the final eigenvalue, and therefore we conservatively estimate the statistical error for each point separately as

$$\sigma_\alpha^{\text{stat}}(n) \equiv 100 \times \Delta E_\alpha(n). \tag{40}$$

Given that these individual statistical errors may be correlated, we define the statistical error of the overall fit as

Table 2. Transition energies $E_\alpha(\infty)$ for methane calculated with 12-state-averaged MCSCF using the sinc DVR basis, for two grid resolutions, calculated by extrapolating to infinite basis size using the method of Section 3.6.

$\Delta =$	$0.39495414a_0$	0.19747707
T	9.666150(1)eV	9.5353(5)
E	10.718654(3)	10.6309(2)
T	10.772476(3)	10.6826(2)
T	10.773745(3)	10.6850(2)

the average of them,

$$\sigma_\alpha^{\text{stat}} \equiv \frac{1}{N_C}\sum_{j=1}^{N_C}\sigma_\alpha^{\text{stat}}(n_j) \tag{41}$$

In summary, we conservatively define the variance in the fitted asymptote, the variance in fitted value of the transition energy in the limit of infinite basis size, as

$$\sigma_\alpha^2 \equiv \left(\sigma_\alpha^{\text{sys}}\right)^2 + \left(\frac{100}{N_C}\sum_{j=1}^{N_C}\Delta E_\alpha(n_j)\right)^2 \tag{42}$$

Furthermore, we perform two calculations with different values of the parameters n_{big} and n_{small} in order to check the error due to the approximations made in our calculation of the Coulomb matrix elements. The significant figures reported in Sections 3.7 and 3.8 agree for the two choices $(n_{\text{big}}, n_{\text{small}}) = (248,31)$ and $(195,39)$.

3.7. Methane excitation energies

We calculate excitation energies of methane using the same nine-orbital full-configuration-interaction representation used for the time-dependent calculations above, using two. The calculation we perform is called state-averaged multiconfiguration self-consistent field (MCSCF) and consists of minimising the average energy of the first 12 electronic states of methane with respect to variations both of the coefficients of the sinc DVR basis functions comprising the nine orbitals, and of the coefficients of the spin-adapted linear combinations of Slater determinants.

These energies are calculated as a function of grid resolution, independent of box size (points on a side n), but with error bars that are due to finite box size calculations, using the method described in the subsection immediately above, and reported in Table 2. Nine or eight calculations are used for the extrapolation to infinite basis size, respectively: for Δ=0.39495414a_0, n = 105, 115, ...185; for Δ=0.19747707, n = 135, 145, 155, ...215.

Table 3. 12-state-averaged MCSCF energies calculated with Gaussian basis sets, aug-cc-pvdz, aug-cc-pvtz, and aug-cc-pvqz, either the full Cartesian basis (no extension) or contracting them spherically (extension -s above).

	DZ-s	DZ	TZ-s	TZ	QZ-s	QZ
T	9.5845	9.5828	9.5381	9.5359	9.5197	9.5160
T	10.8820	10.8815	10.7792	10.7774	10.7462	10.7419
E	10.9799	10.9795	10.8225	10.8173	10.7585	10.7517
T	11.0339	11.0335	10.8792	10.8740	10.8157	10.8089

For comparison, we perform the same state-averaged MCSCF calculations using Gaussian basis sets, using the Columbus suite of codes for quantum chemistry [47]. We use three basis sets, aug-cc-pvdz, aug-cc-pvtz and aug-cc-pvqz [48], using either the full set of Cartesian basis functions or contracting them to make spherical harmonics. These results are reported in Table 3.

There are only two columns in Table 2, for only one molecule; any conclusions about the method at this stage must be considered preliminary. The columns in Table 2, the results with the current sinc basis, differ consistently by about 0.1eV. The double-zeta and triple-zeta columns in Table 3, obtained with standard Gaussian basis set methods, have a range of differences, from 0.05 to 0.16eV. Therefore, it appears that rougly double-zeta accuracy is obtained with a grid spacing Δ=0.39495414a_0, and roughly triple-zeta accuracy is obtained with Δ=0.19747707. We perform a more quantitative analysis of the performance of the representation as a function of grid resolution Δ in the next section, on cubane.

3.8. Cubane (C_8H_8) ionisation potential

As presently described, without elaboration, this representation for electronic wave functions of molecules using the sinc DVR requires that nuclei be placed on the Cartesian grid points and as such, has limited applicability. In the conclusion, we speculate about elaborations to the method that would allow it to calculate a molecule in an arbitrary internuclear geometry.

For the moment, the cubane molecule provides a good test of the method due to its cubic geometry. Not only is it cubic, but the C–C and H–H distances are approximately in the ratio 9:5 or 1.8. The theoretical equilibrium geometry calculated at the coupled cluster with single and double excitations (CCSD) using the cc-pVDZ Dunning basis set [48], as tabulated by NIST [49], has the carbons at $x, y, z = \pm 0.7893$ Angstrom and the hydrogens at 1.4248 Angstrom, a ratio of 1.805. So we take the geometric average of these distances, and multiply and divide by the square root of 1.8, to arrive at our geometry, with the

Table 4. Ionisation potentials of cubane, in electronvolts, as described in the text.

	$^2T_{2g}$		$^2T_{2u}$	
Resolution	IP	KIP	IP	KIP
0.5974764	9.84027(1)	10.68006(1)	10.24536(2)	11.16661(2)
0.2987382	9.69775(2)	10.54452(50)	9.84952(2)	10.79933(40)
0.1493691	9.63852(10)	10.47702(10)	9.69365(4)	10.64553(4)
0	9.591(2)	10.433(5)	9.560(9)	10.523(3)

carbons at $x, y, z = \pm 1.493691 a_0$ (approximately 0.7904 Angstrom) and the hydrogens at $x, y, z = \pm 2.6886438 a_0$ (approximately 1.4228 Angstrom). We use three grid resolutions, $\Delta = 0.5974764$, 0.2987382 and $0.1493691 a_0$.

In Table 4, we present results showing the first two ionisation potentials of cubane in the Hartree–Fock approximation, calculated as in Section 3.6, extrapolated to infinite basis size, for the three grid spacings Δ. These infinite-basis results are then extrapolated to $\Delta = 0$, and that result is shown in the fourth row of the table. The method that we use for this final extrapolation is described later in this section.

Two potentials are reported, both those corresponding to the difference between the fully converged Hartree–Fock energies of the neutral and cation, labelled 'I.P.' in Table 4, and those corresponding to the Koopman's ionisation potential, labelled 'K.I.P.', corresponding to the neutral Hartree–Fock highest occupied molecular orbital energies, calculated as the difference between the neutral Hartree–Fock energy and the cation energy obtained through diagonalisation using the neutral Hartree–Fock orbitals. The precision obtained in the latter is much lower than the former due to the primitive Hartree–Fock implementation we use. Five or six points are used for the extrapolation to infinite basis size; for resolution $\Delta = 0.5974764 a_0$, $n = 64$, 72, 80, 90, 108; for $\Delta = 0.2987382$, $n = 81$, 91, 99, 105, 117; and for $\Delta = 0.1493691 a_0$, $n = 185$, 195, 205, 215, 225 and 235.

However, the precision in the results for cubane in Table 4 does not come from the extrapolation. For the ionisation potentials (I.P.) the precision comes from disagreement between the two calculations for the different choices for n_{big} and n_{small}; for the Koopman's ionisation potentials (K.I.P.), the precision comes from nonconvergence of the primitive Hartree–Fock procedure, and our conservative choice for the definition of statistical error based upon it.

The ionisation potentials of cubane have been previously calculated in Refs. [50–52]. The lowest T_{2g} and T_{2u} Koopmans' ionisation potentials, exactly analogous to those reported here, were calculated to be 10.39 and 10.58eV, respectively, at the double zeta with polarisation level of theory, in Ref. [52]. In a different basis, the K.I.P.s were 10.42 and 10.59eV, and the delta-SCF result, closely comparable to the I.P. reported here, was 9.74eV for both the T_{2g} and T_{2u} states. In Ref. [51], the Koopmans' I.P.s were calculated as 10.40 and 10.62eV, respectively, and the I.P.s were calculated to be 9.38 and 9.73eV at a higher level of theory with more correlation.

By comparing these numbers from the literature to those in Table 4, it seems that the present representation will be able to produce qualitatively accurate results on polyatomic molecules using a grid spacing of approximately $0.3 a_0$, the medium resolution in the table. At this medium resolution, it seems that double-zeta quality transition energies are obtained; stepping up to the finest resolution produces improvements of less than 0.1eV for the lower cation ionisation potential, and improvements slightly greater for the higher I.P. This accuracy of 0.1eV is unsatisfactory for many applications involving ground-state Born–Oppenheimer dynamics; the standard called for there, 'chemical accuracy', is one kilocalorie per mole [35], which is approximately 43meV. Examining the lowest-resolution results, one can see that errors introduced going from the resolution of approximately $\Delta = 0.3 a_0$ to $0.6 a_0$ are a substantial fraction of an electron volt. The accuracy at $0.6 a_0$ is probably unsatisfactory for almost all applications, but $\Delta = 0.3 a_0$ seems sufficient for qualitative studies of excited state potential energy curves and time-dependent electron dynamics of polyatomic molecules.

We have attempted to quantify the performance more accurately by extrapolating the results in the first three rows of Table 4 to $\Delta = 0$. The power law for the error that was observed for the one electron results and reported above – a power law $\Delta^{2.13}$ for the error – does not fit the results on cubane in Table 4. Unfortunately, the exponent in the power law for these cubane results is significantly lower. In order to obtain error bars on the predicted extrapolation, we fit the four columns of Table 4 to the same power law. In other words, we consider the columns in the table to be labelled $E_i(\Delta)$, and with these 12 points fit the nine parameters $\{e_1 \ldots e_4, b_1 \ldots b_4, Q\}$ in the functional form

$$E_i(\Delta) = e_i + b_i \Delta^Q \tag{43}$$

using this fit, we obtain the power law exponent $Q = 1.205 \pm 0.18$. The error bars in the final row of Table 4, showing this extrapolation, are almost entirely due to the error of this fit, and not to the error of the points used in the fit.

Using the values of b_i from this fit, we obtain the value at which the accuracy of the computed ionisation potentials for cubane is one kilocalorie per mole or 43meV, also known as 'chemical accuracy' [35]. By solving $0.043 = b_i \Delta^{1.205}$, in electronvolts, for Δ,

given the fitted b_i, we obtain $\Delta = 0.139a_0$ from both the I.P. and the K.I.P. of the lower ($^2T_{2g}$) state, and approximately $\Delta = 0.06a_0$ for both I.P. and K.I.P. for the upper ($^2T_{2u}$) state. The average of these values is about 0.1 bohr. Given the flexibility of the representation, it seems reasonable to expect that chemical accuracy will be obtained generally, for other molecules as well, at this resolution. In the conclusion, we mention improvements to the method that would account for the truncation of the basis in momentum space and that would hopefully yield chemical accuracy with an even lower resolution.

4. Conclusion

We have demonstrated an efficient real-space basis set representation for electronic structure using sinc basis functions, a generalisation of the method of Ref [1] to Cartesian coordinates. This and that method make use of a resolution-of-the-identity approximation to arrive at diagonal expressions for the one- and two-electron matrix elements. The singular Coulomb potential is discarded and the one- and two-electron matrix elements are obtained instead from the kinetic energy matrix elements by requiring that the relationship between the Coulomb potential and Laplace operator – that the former is the Green's function of the latter – be maintained in their numerical matrix representations. The normally forth-rank tensor of two-electron matrix elements is rendered first-rank, and may be stored in memory for even the largest problems. The energies and virial theorem ratios calculated are far superior to those obtained with the variational method using the same sinc basis.

We note that this DVR representation bears similarity to that of Ref. [53], a 3D treatment for atoms in spherical coordinates. The 3D representations, the present one and that of Ref. [53], as opposed to the treatment for spherical coordinates in Ref. [1] in which only the radial coordinate is discretised, permit the maximum degree of parallel computer scalability. We also note that a similar *ansatz* involving the kinetic energy operator has been applied to Gaussian basis functions in Ref. [54].

The representation described in this paper may provide a foundation for an efficient treatment of electronic structure that would compete with Gaussian basis set methods in applications for which chemical accuracy [35] is required. With this goal in mind, several easy-to-implement elaborations that would improve its performance are conceivable. For instance, it is desirable to have grids with different resolutions for different electrons in the Slater determinant basis, such that different orbitals with different spatial extents can be described efficiently. Algebra along these lines is presented the Appendix. Also, effective theory [55] may be used to account for the truncation in momentum space and improve the convergence of the results with respect to resolution Δ.

However, the most important improvement is to permit small grid distortions. Presently, the method requires that nuclei only be placed on the Cartesian grid points, which is its most major limitation. If the grid could be distorted slightly, but arbitrarily, then arbitrary internuclear geometries could be calculated simply by distorting the grid such that the grid points and nuclei coincide. Furthermore, if these distortions could be made complex-valued, then the representation would be capable of calculating ionisation using the method of complex coordinate scaling [56–60].

Implementing complex-valued grid distortions is, therefore, the next step in the development of this real-space representation for electronic structure. Including grid distortions in the method will permit arbitrary fixed-nuclei geometries and the accurate representation of ionisation. It will also enable calculations of fully nonadiabatic electronic and nuclear dynamics of polyatomic molecules subject to intense, ultrafast laser light, with the open-source implementation published in Refs. [41,61,62]. Because of its efficiency and uniform resolution, this sinc DVR for electronic structure is best suited to highly correlated, highly excited dynamics of electrons in molecules, not ground-state electronic structure. With the method of Domcke and coworkers [63–65], we are using it to calculate phase matched signals for wave mixing experiments on polyatomic molecules, and we look forward to this and other applications in the future.

Acknowledgments

We thank the National Energy Research Scientific Computing Center (NERSC) for computational resources.

Disclosure statement

No potential conflict of interest was reported by the authors.

Funding

This work was supported by the US Department of Energy Office of Basic Energy Sciences, Division of Chemical Sciences [Grant Number DE-AC02-05CH11231]; US Department of Energy [Grant Number DESC0007182].

References

[1] C.W. McCurdy, M. Baertschy, and T.N. Rescigno, J. Phys. B **37**, R137 (2004).

[2] R.M. Parrish, E.G. Hohenstein, N.F. Schunck, C.D. Sherrill, and T.J. Martinez, Phys. Rev. Lett. **111**, 132505 (Sep 2013).
[3] E.G. Hohenstein, R.M. Parrish, and T.J. Martinez, J. Chem. Phys. **137**, 044103 (2012).
[4] R.M. Parrish, E.G. Hohenstein, T.J. Martinez, and C.D. Sherrill, J. Chem. Phys. **137**, 224106 (2012).
[5] E.G. Hohenstein, R.M. Parrish, C.D. Sherrill, and T.J. Martinez, J. Chem. Phys. **137**, 221101 (2012).
[6] U. Benedikt, A.A. Auer, M. Espig, and W. Hackbusch, J. Chem. Phys. **134**, 054118 (2011).
[7] A.S. Dickinson and P.R. Certain, J. Chem. Phys. **49**, 4209 (1968).
[8] J.V. Lill, G.A. Parker, and J.C. Light, Chem. Phys. Lett. **89**, 483 (1982).
[9] J.C. Light, I.P. Hamilton, and J.V. Lill, J. Chem Phys. **82**(3), 1400 (1985).
[10] G.C. Corey and D. Lemoine, J. Chem. Phys. **97**(6), 4115 (1992).
[11] C. Leforestier, J. Chem. Phys. **101**(9), 7357 (1994).
[12] G.C. Corey and J.W. Tromp, J. Chem. Phys. **103**, 1812 (1995).
[13] O.A. Sharafeddin and J.C. Light, J. Chem. Phys. **102**, 3622 (1995).
[14] V. Szalay, J. Chem. Phys. **105**, 6940 (1996).
[15] S. Sukiasyan and H.-D. Meyer, J. Phys. Chem. A **105**, 2604 (2001).
[16] R.G. Littlejohn and M. Cargo, J. Chem. Phys. **117**(1), 27 (2002).
[17] H.-G. Yu, J. Chem. Phys. **122**, 164107 (2005).
[18] P.J. Davis, *Circulant Matrices* (American Mathematical Soc., New York, NY, 1979).
[19] J. Chen and T.L. Li, Procedia Comput. Sci. **18**, 571 (2013).
[20] T. Torsti, T. Eirola, J. Enkovaara, T. Hakala, P. Havu, V. Havu, T. Höynälänmaa, J. Ignatius, M. Lyly, I. Makkonen, T.T. Rantala, J. Ruokolainen, K. Ruotsalainen, E. Räsänen, H. Saarikoski, and M.J. Puska, Phys Status Solidi (b) **243**(5), 1016 (2006).
[21] A.P. Seitsonen, M.J. Puska, and R.M. Nieminen, Phys. Rev. B **51**, 14057 (May 1995).
[22] F. Ancilotto, P. Blandin, and F. Toigo, Phys. Rev. B **59**, 7868 (Mar 1999).
[23] J.R. Chelikowsky, N. Troullier, and Y. Saad, Phys. Rev. Lett. **72**, 1240 (Feb 1994).
[24] S.R. White, J.W. Wilkins, and M.P. Teter, Phys. Rev. B **39**, 5819 (Mar 1989).
[25] J.E. Pask, B.M. Klein, C.Y. Fong, and P.A. Sterne, Phys. Rev. B **59**, 12352 (May 1999).
[26] T.A. Arias, Rev. Mod. Phys. **71**, 267 (Jan 1999).
[27] F.L. Yip, C.W. McCurdy, and T.N. Rescigno, Phys. Rev. A **81**, 053407 (May 2010).
[28] T.N. Rescigno and C.W. McCurdy, Phys. Rev. A **62**, 032706 (Aug 2000).
[29] D.T. Colbert and W.H. Miller, J. Chem. Phys **92**, 1982 (1992).
[30] D.K. Jordan and D.A. Mazziotti, J. Chem. Phys. **120**(2), 574 (2004).
[31] D.A. Mazziotti, J. Chem. Phys. **117**(6), 2455 (2002).
[32] L. Füsti-Molnár and P. Pulay, J. Chem. Phys. **117**(17), 7827 (2002).
[33] L. Füsti-Molnár, J. Chem. Phys. **119**(21), 11080 (2003).
[34] A.V. Scherbinin, V.I. Pupyshev, and N.F. Stepanov, Int. J. Quantum Chem. **60**, 843 (1996).
[35] P.A. Bash, L.L. Ho, J.A.D. MacKerrell, D. Levine, and P. Hallstrom, Proc. Natl. Acad. Sci. USA **93**, 3698 (1996).
[36] F. Stenger, *Numerical Methods Based on Sinc and Analytic Functions*. (Springer, New York, NY, 1993).
[37] G.C. Groenenboom and D.T. Colbert, J. Chem. Phys. **99**, 9681 (1993).
[38] D.J. Haxton, J. Phys. B **40**, 4443 (2007).
[39] J. Dongarra, P. Koev, and X. Li, in *Templates for the Solution of Algebraic Eigenvalue Problems: A Practical Guide*, edited by Z. Bai, J. Demmel, J. Dongarra, A. Ruhe, and H. van der Vorst. (SIAM, Philadelphia, 2000), pp. 324–326.
[40] L. Tao, C.W. McCurdy, and T.N. Rescigno, Phys. Rev. A **79**, 012719 (Jan 2009).
[41] D.J. Haxton, K.V. Lawler, and C.W. McCurdy, Phys. Rev. A **83**, 063416 (2011).
[42] R. van Harrevelt, J. Chem. Phys. **125**, 124302, 2006.
[43] D.J. Haxton and C.W. McCurdy, Phys. Rev. A **90**, 053426 (2014).
[44] A.M. Mebel, S.-H. Lin, and C.-H. Chang, J. Chem. Phys. **106**, 2612 (1997).
[45] R. van Harrevelt, J. Chem. Phys., **126**, 204313 (2007).
[46] M.D. Lodriguito, G. Lendvay, and G.C. Schatz, J. Chem. Phys. **131**, 224320 (2009).
[47] H. Lishka, R. Shepard, I. Shavitt, R.M. Pitzer, M.D. os, T. Muller, P.G. Szalay, F.B. Brown, R. Ahlrichs, H. . J. Bohm, A. Chang, D.C. Comeau, R. Gdanitz, H. Dachsel, C. Ehrhardt, M. Ernzerhof, P. Hochtl, S. Irle, G. Kedziora, T. Kovar, V. Parasuk, M.J.M. Pepper, P. Scharf, H.S. and M. Schindler, M. Schuler, M. Seth, E.A. Stahlberg, J.-G.Z. ao, S. Yabushita, Z. Zhang, M. Barbatti, S. Matsika, M.S. uurmann, D.R. Yarkony, S.R. Brozell, E.V. Beck, and J.-P.B. audeau, Columbus, an ab initio electronic structure program. 2006. Release 5.9.1.
[48] J.T.H. Dunning J. Chem. Phys. **90**, 1007 (1989).
[49] "Nist standard reference database number 101, release 16a," in *NIST Computational Chemistry Comparison and Benchmark Database*, edited by R.D.J. III. (National Institute of Standards and Technology, Gaithersburg MD, 20899, 2013).
[50] J.M. Schulman, C.R. Fischer, P. Solomon, and T.J. Venanzi, J. Am. Chem. Soc. **100**(10), 2949 (1978).
[51] V. Galasso, Chem. Phys. **184**(1–3), 107 (1994).
[52] V. Zakrzewski and J. Ortiz, Chem. Phys. Lett. **230**(3), 313 (1994).
[53] F. Robicheaux, J. Phys. B. **45**, 135007 (2012).
[54] D.S. Lambrecht, K. Brandhorst, W.H. Miller, C.W. McCurdy, and M. Head-Gordon, J. Phys. Chem. A **115**(13), 2794 (2011).
[55] G. Lepage. *How to Renormalize the Schrodinger Equation*. (Cornell University, Ithaca, NY, 1997), pp. 135–180.
[56] J. Aguilar and J.M. Combes, Commun. Math. Phys., **22**, 269 (1971).
[57] E. Balslev and J.M. Combes, Commun. Math. Phys., **22**, 280 (1971).
[58] N. Moiseyev, P.R. Certain, and F. Weinhold, Mol. Phys. **36**, 1613 (1978).
[59] N. Moiseyev and J.O. Hirschfelder, J. Chem. Phys., **88**, 1063 (1987).
[60] W. Reinhardt, Ann. Rev. Phys. Chem., **33**, 223 (1982).

[61] D.J. Haxton and C.W. McCurdy, Phys. Rev. A, **91**, 012509 (Jan 2015).
[62] D.J. Haxton, C.W. McCurdy, T.N. Rescigno, K.V. Lawler, J. Jones, B. Abeln, and X. Li. LBNL-AMO-MCTDHF.
[63] L. Seidner, G. Stock, and W. Domcke, J. Chem. Phys. **103**, 3998 (1995).
[64] S. Meyer and V. Engel, Appl. Phys. B, **71**, 293 (2000).
[65] H. Wang and M. Thoss, Chem. Phys., **347**, 139 (2008).
[66] J.S. Sims and S.A. Hagstrom, J. Chem. Phys. **124**, 094101 (2006).

Appendix A. Derivation for different electron one and electron two bases

It is wasteful to define orbitals all in the same basis extending over the entire molecule. Many electrons, notably core electrons, will be localised. To account for this, it is imperative to define orbitals on different grids with different spatial extent and resolution. Such a treatment then calls for Slater determinants belonging to different classes containing different numbers of electrons occupying orbitals belonging to different grids. However, since the one electron bases are not combined, there is no problem of linear dependence nor any significant issue related to orthogonality.

One could, for example, interpolate the density on the sparser grid onto the finer grid, then use T^{-1} for the finer grid to evaluate the integral. However, it is interesting to try to adapt the derivation directly to the case of two different bases.

The derivation with two different bases for electrons one (ij) and two (kl) follows. We define

$$y^{kl}(\vec{r}_1) = \int d^3\vec{r}_2\, \chi_k^{(2)}(\vec{r}_2)\chi_l^{(2)}(\vec{r}_2)\frac{1}{|\vec{r}_1 - \vec{r}_2|} \tag{A1}$$

Applying the Laplacian to both sides of Equation (A1) and approximating $y^{kl}(\vec{r}_1)$ as a linear combination of the basis functions in $\vec{r}_2$,

$$y^{kl}(\vec{r}_1) \approx \sum_{\text{ALL } n} y_n^{kl}\chi_n^{(2)}(\vec{r}_1), \tag{A2}$$

applying the Laplacian with respect to $\vec{r}_1$ to this expansion, multiplying through by $\chi_m^{(1)}(\vec{r}_1)$, integrating over $\vec{r}_1$ and equating the results leads to

$$\sum_n y_n^{kl} T_{mn} = 2\pi \int d^3\vec{r}\, \chi_k^{(2)}(\vec{r})\chi_l^{(2)}(\vec{r})\chi_m^{(1)}(\vec{r}) \tag{A3}$$

where $T_{mn} = -\frac{1}{2}\langle\chi_m^{(1)}|\nabla^2|\chi_n^{(2)}\rangle$ are the kinetic energy matrix elements.

Again using the resolution of the identity to approximate the density (sum of squares of basis functions), the right-hand side of Equation (20) is evaluated as

$$\sum_n y_n^{kl} T_{mn} = 2\pi\,\Delta_{(2)}^{-3/2}\delta_{kl}S_{km} \tag{A4}$$

with S the overlap matrix

$$S_{lm} = \int d^3\vec{r}\, \chi_l^{(2)}(\vec{r})\chi_m^{(1)}(\vec{r}) \tag{A5}$$

giving

$$y_n^{kl} = 2\pi\,\Delta_{(2)}^{-3}\delta_{kl}\sum_m S_{mn}(T^{-1})_{mk}. \tag{A6}$$

Using these coefficients and inserting Equation (A2) into 14 gives the expression for the two-electron matrix elements

$$[ij|kl] = \sum_n y_n^{kl}\int d^3\vec{r}_1\, \chi_i^{(1)}(\vec{r}_1)\chi_j^{(1)}(\vec{r}_1)\chi_n^{(2)}(\vec{r}_1). \tag{A7}$$

Once again, the integral on the RHS is evaluated by a resolution of the identity, this time in the r_1 density, to obtain the expression

$$[ij|kl] = 2\pi\,(\Delta_{(1)}\Delta_{(2)})^{-3/2}\delta_{ij}\delta_{kl}\sum_{mn} S_{in}S_{mk}T_{nm}^{-1}. \tag{A8}$$

Because the electron one and electron two grids do not commensurate, more than one column (equivalently, with different indexing, one row) of T^{-1} will have to be stored.